metals

Article

Fracture Behavior of Hadfield Cast Steels Exposed to Impact Loading

Aleksandar Vukosavljević [1], Aleksandar Sedmak [2], Stefan Dikić [1,*], Ljubica Radović [3] and Nenad Radović [1]

[1] Faculty of Technology and Metallurgy, University of Belgrade, 11000 Belgrade, Serbia
[2] Faculty of Mechanical Engineering, University of Belgrade, 11000 Belgrade, Serbia
[3] Military-Technical Institute, 11030 Belgrade, Serbia
* Correspondence: sdikic@tmf.bg.ac.rs

Abstract

Impact toughness of three different samples was evaluated using an instrumented Charpy pendulum combined with fractography performed using scanning electron microscopy (SEM) to analyze the effects of heat treatment and vanadium as alloying element. Samples were made from Mn16V with water quenching and aging (WQA), as well as from Mn16V and Mn16 with WQA and additional aging (WQAA). It was concluded that vanadium reduced impact toughness, whereas the additional aging had practically no effect.

Keywords: Hadfield steel; cast steel; fracture; quenching; aging; toughness

1. Introduction

Hadfield manganese steel is used in excavator components, crusher segments, and machine parts that must be resistant to impact loading, except for wear and abrasion [1–3]. Therefore, impact toughness should be sufficient, in addition to high resistance to wear and abrasion. One should note that the unique set of mechanical properties of Hadfield steel is achieved through the strain hardening effect resulting from the austenite-to-martensite transformation [4–7]. This phenomenon was explained in [4], where Powell, Marshall, and Backofen discuss the significant strain hardening in austenitic steels, particularly the multi-stage hardening resulting from deformation-induced martensite formation. Later on, Dastur and Leslie analyzed the mechanism of strain hardening in Hadfield manganese steel [5]. Similar analysis was performed in [6,7] to get the full picture of this mechanism.

One should notice that Hadfield steel in as-cast state contains carbides and dendrites, which reduce its toughness, so they should be eliminated or at least reduced through appropriate heat treatment, as shown in Figure 1, involving high-temperature dissolution and fast cooling [8–10]. Metallographic and microstructural effects are described in [8], while the effect on mechanical properties is shown in [9], where it was pointed out that optimized heat treatment is of crucial importance in terms of dissolution temperature and time, as well as the cooling rate. Critical cooling rate necessary to avoid carbide precipitation during quenching of austenitic manganese steel was investigated in [10] to provide an efficient heat treatment analysis program and probability of carbide precipitation during quenching through the finite difference method.

Check for updates

Academic Editor: Dariusz Rozumek

Received: 27 January 2026
Revised: 27 February 2026
Accepted: 2 March 2026
Published: 5 March 2026

Copyright: © 2026 by the authors. Licensee MDPI, Basel, Switzerland. This article is an open access article distributed under the terms and conditions of the Creative Commons Attribution (CC BY) license.

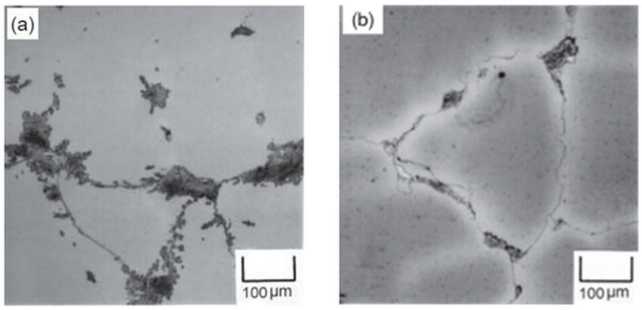


Figure 1. Microstructure with carbides on grain boundaries [10]: (**a**) as-cast (**b**) after heat treatment [10]. Reprinted from ref. [10] (Following CC BY-NC 4.0).

Another important issue here is alloying, as described in [11–16]. The effect of vanadium on the mechanical properties and microstructure of high manganese steel was analyzed in [11–14], indicating an increase in hardness and wear resistance, as well as reduction in impact toughness. The increase in hardness and wear resistance of the alloys occurred due to vanadium carbides, especially due to their size and distribution. Microstructural changes due to heat treatment and alloying additions of vanadium (1–2%) and copper (1%) were studied in [15]. The outstanding effect of specially designed heat treatment was attributed to fine carbide precipitates produced by the migration and growth of "vanadium–vacancy" clusters. In [16], the effects of carbon and manganese content, along with additions of molybdenum, chromium, and vanadium, on the microstructure and mechanical properties of Hadfield steel were analyzed. It was found that these elements alter phase balance and density, thereby influencing the material's overall characteristics for better wear resistance, but the effect of vanadium was not clearly specified, because the amounts used in this study were small and originated from the charge rather than being purposely put into the melt, since it was thought that higher content would form carbides difficult to dissolve. In [17], proper heat treatment cycle, typical mechanical properties, and work hardening rate of Hadfield steel was discussed, so as to know which application the steel is best suited for. The re-aging [13] effect on Hadfield steel properties was examined, indicating benefits to mechanical properties.

As already mentioned, so-called water quenching (WQ) at high temperatures is used to dissolve carbides and transform dendrites, followed by aging, which is one of the aims of this investigation. In the scope of the broader investigation, three different heat treatments were applied to four different chemical compositions of Hadfield steel in order to examine their effects on impact toughness, which was identified as the most critical property according to previous research [18]. In this way, the effect of chemical composition (Mn, V) and heat treatment was obtained [19], where these effects were presented in terms of hardness and strength. Nevertheless, the focus here was on the effect on toughness of the additional aging and content of vanadium, which has not been covered in the literature, at least to the best knowledge of these authors. Although these effects are analyzed and explained in respect to microstructure, tensile properties and hardness, effects on impact, and/or fracture toughness are not covered. Therefore, in this research, the impact toughness of four different samples was evaluated on an instrumented Charpy pendulum and combined with micrography and fractography performed through SEM. In this way, a deeper insight of the effect of heat treatment and V on impact toughness was enabled. Based on these findings and conclusions, recommendations for the use of investigated Hadfield steel can be given.

2. Materials and Methods

2.1. Materials

Two high-manganese austenitic Hadfield steels were investigated in this study: Mn16 and Mn16V. The Mn16V grade contains vanadium as a microalloying element intended to promote carbide precipitation during post-quenching aging. Chemical compositions of tested steels are shown in Table 1. All samples were subjected to solution treatment followed by water quenching (WQ). Additionally, selected specimens were exposed to single-stage aging (WQA) and double-stage aging (WQAA), according to the thermal cycles schematically presented in Figure 2.

Table 1. Chemical composition of Hadfield steels used here.

	%C	%Si	%Mn	%P	%S	%Cr	%Ni	%Mo	%V
Mn16	1.08	0.60	14.11	0.059	0.0023	2.40	0.149	0.043	-
Mn16V	1.18	0.60	14.49	0.043	0.0005	2.05	0.044	0.015	0.475

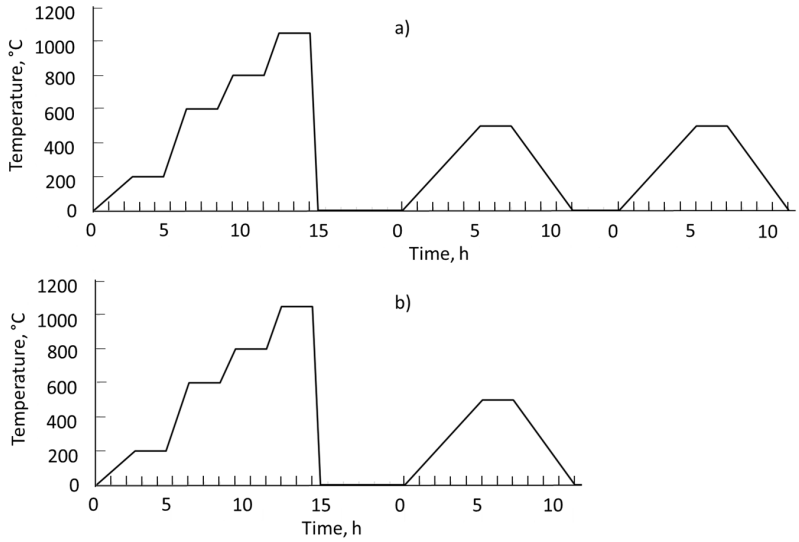


Figure 2. Heat treatment: (**a**) quenching and aging; (**b**) quenching and double aging.

The specimens were first solution-treated at 1050 °C and held for 2 h to promote chemical and microstructural homogenization and to evaluate the effect of a relatively short annealing time on the resulting steel properties. Heating to 1050 °C was carried out using a controlled, stepwise regime with intermediate isothermal holds at approximately 200 °C, 600 °C, and 800 °C prior to the final ramp to the solution-treatment temperature (Figure 2). This multi-stage heating schedule was intentionally selected to enhance thermal uniformity, facilitate progressive diffusion processes, and minimize internal thermal stresses, thereby improving the efficiency of homogenization within the limited soaking time.

Immediately after the 2 h soaking period, the specimens were water-quenched to room temperature in order to retain a fully austenitic microstructure and suppress premature carbide precipitation (WQ condition). This rapid quenching step was essential to preserve the high-temperature solid-solution state achieved during solution treatment, enabling a reliable assessment of the homogenization effect and its influence on subsequent steel properties.

Subsequently, the selected specimens were subjected to artificial aging treatments. In the single-aging condition (WQA), the water-quenched samples were reheated to an intermediate temperature of 500 °C and held for 2 h, followed by cooling to room temperature. This treatment was intended to promote controlled precipitation within the austenitic matrix. In the Mn16V steel, aging is expected to induce the formation of fine vanadium

carbides (VC), whereas in Mn16 steel precipitation occurs primarily in the form of Fe–Mn–C carbides due to the absence of vanadium. The effect of heat treatment on hardness is shown in Table 2. The initial value of hardness was around 200 HV.

Table 2. Hardness of Hadfield steels, Mn16 and Mn16V.

Material	Hardness WQ (HV)	Hardness WQA (HV)
Mn16	228.6	242.5
Mn16V	242.4	269.7

In addition, a double-aging treatment (WQAA) was applied to part of samples that had previously been subjected to aging, both for Mn16 and Mn16V steels. Double-aged samples underwent the same thermal cycle as they did during the first aging phase. The samples were placed into in a cold furnace and heated together in a furnace to the aging temperature of 500 °C. After 2 h at the aging temperature, the furnace was switched off, and the samples were cooled in the furnace with the door open. The double-aging route was designed to intensify and homogenize the precipitation processes within the austenitic matrix, enabling the evaluation of the combined effects of vanadium addition and repeated aging on the microstructural evolution and resulting mechanical properties.

2.2. Impact Testing on Charpy Instrumented Pendulum

Standard Charpy specimens of a square cross-section (10 × 10 mm) containing 2 mm deep 45° V notch with 0.25 mm root radius were used. The specimen is supported as a beam in a horizontal position and loaded behind the notch by the impact of a heavy swinging pendulum (Figure 3), with the impact velocity of approximately 5 m/s [17]. The testing of three specimens per sample was performed. The test was performed using the SCHENCK TREBELL 150/300 J instrumented Charpy pendulum (Instron GmbH, Im Birkenstock 15, 65451 Kelsterbach, Germany). Device calibration is performed once a year.

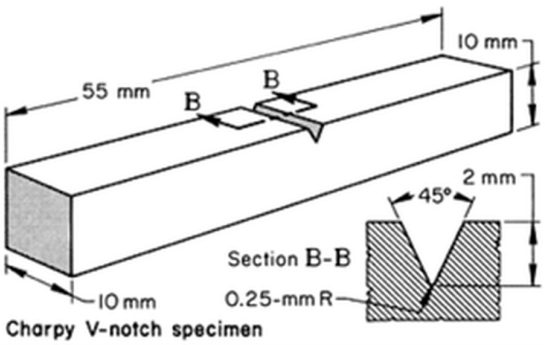


Figure 3. Charpy V notch standard specimen [17]. Reprinted with permission from ref. [17]. 2014, World Foundry Organization Ltd.

The energy absorbed during fracture, in joules (J), often designated KV, is read directly from a calibrated dial on the impact tester.

Additional information regarding material impact toughness can be obtained if the impact tester is instrumented to provide the load time history of the specimen during the test, as shown in Figure 4, enabling the separation of energies for crack initiation and propagation, as described and applied in [20–22]. The energy for crack initiation is defined as the area below the load-time curve to the point of maximum force, while the energy for crack propagation is defined as the remaining are under the load-time curve. To calculate these two energies, one should use the following equation:

$$A = \int_0^{t_1} F(t) \cdot v(t) \cdot dt$$

where $F(t)$ is the force and $v(t)$ is the pendulum speed, which is calculated as follows:

$$v(t) = v_0 + \frac{1}{m} \int_{t_0}^{t} F(t) \cdot dt$$

where m is pendulum mass. Since all mentioned values are known, the energies for crack initiation and propagation are calculated directly through the pendulum.

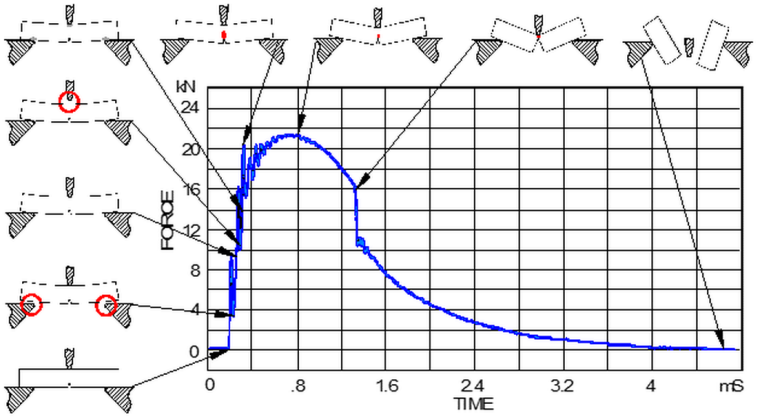


Figure 4. Typical load vs. time record during testing on an instrumented Charpy pendulum [17]. Reprinted with permission from ref. [17]. 2014, World Foundry Organization Ltd.

The results of the instrumented Charpy test can be used for material selection, keeping in mind different material behavior. Namely, for the same load level, the ratio between the energy for crack initiation and its propagation can be quite different, meaning that either initiation or propagation energy can be dominant. Without a deep analysis, it can be noted that higher crack propagation energy is convenient for cast materials, such as Hadfield steel analyzed here, since crack-like defects cannot be excluded.

2.3. Fractography

Fractographic analysis was performed using a scanning electron microscope (SEM, Jeol JSM 6610LV, Tokyo, Japan) at different magnifications. Low-magnification observations were used to identify the overall fracture morphology, the fracture initiation site, and the crack propagation sites. Higher magnifications enabled detailed characterization of micro-mechanisms of fracture features, such as dimples, cleavage facets, secondary cracks, and inclusions, were analyzed to distinguish between ductile and brittle fracture behavior and to identify possible fracture initiation sites. Features such as inclusions, secondary cracks, dimples, micro voids and cleavage facets were analyzed to distinguish between ductile and brittle fracture behavior and to identify possible fracture initiation sites. Fractography was performed on two samples, (4) Mn16V WQA and (7) Mn16 WQAA.

3. Results

3.1. Impact Toughness

Examples of force–time and energy–time diagrams are shown in Figures 5–7, one from each set of samples (marked by 4 for Mn16V with WQA, seven for Mn16 with WQAA and eight for Mn16V with WQAA, respectively), as well as in Figure 8, corresponding to the previously tested sample (3) (Mn16 with WQA [15]). The results for the average values of

initiation and propagation energies, as well as for the total energy, are shown in Table 3, based on the testing of three specimens per sample.

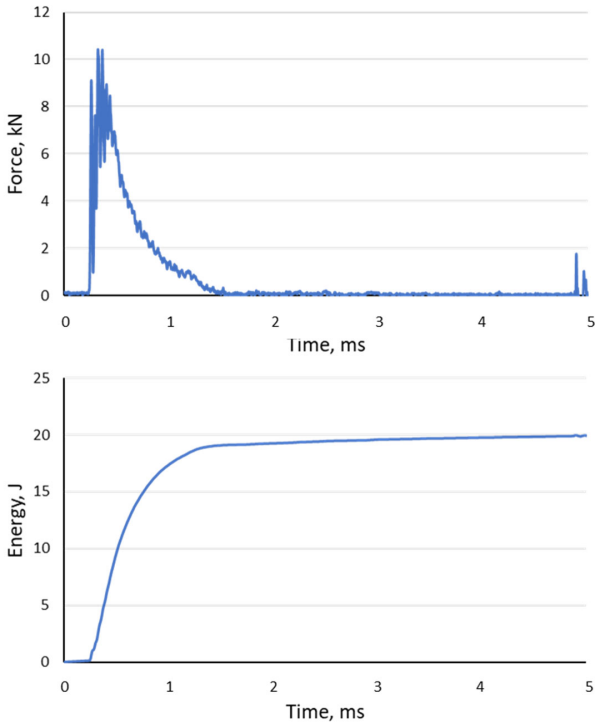


Figure 5. Force–time and energy–time diagrams for sample (4–Mn16V, WQA).

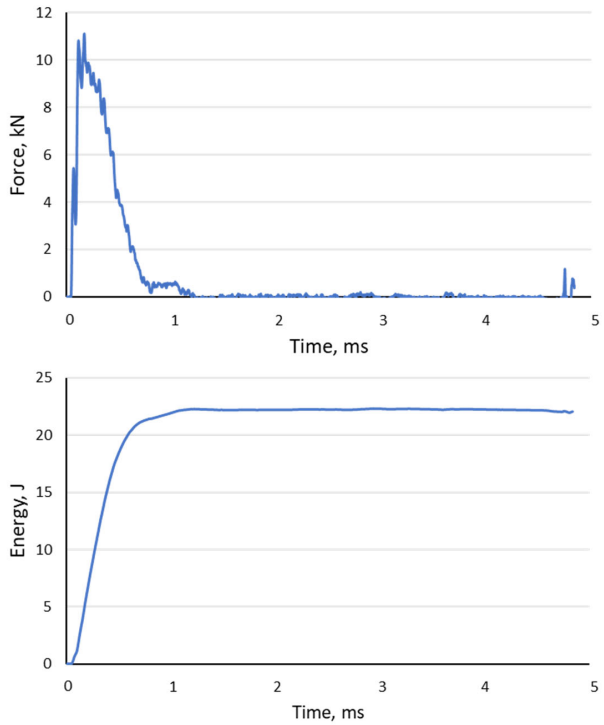


Figure 6. Force–time and energy–time diagrams for sample (7–Mn16, WQAA).

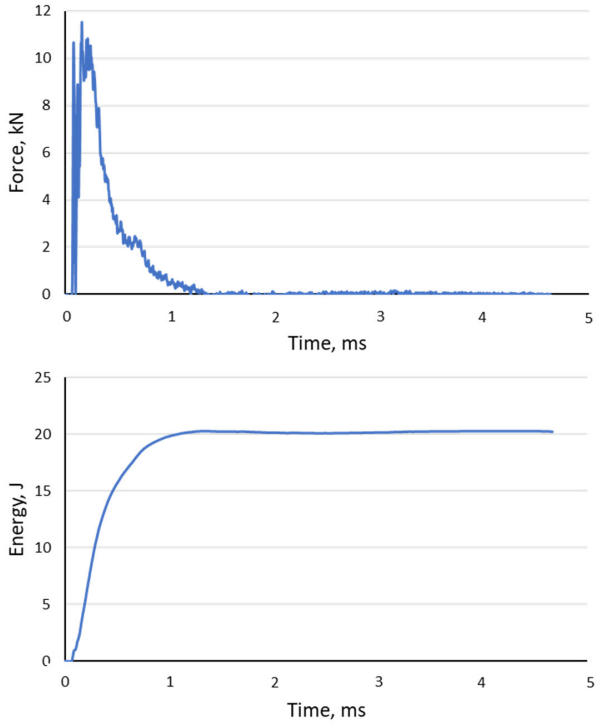


Figure 7. Force–time and energy–time diagrams for sample (8–Mn16V, WQAA).

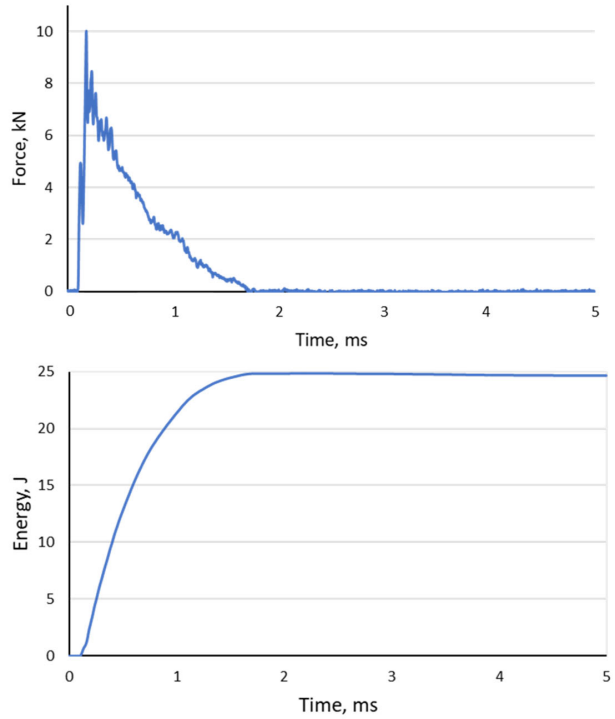


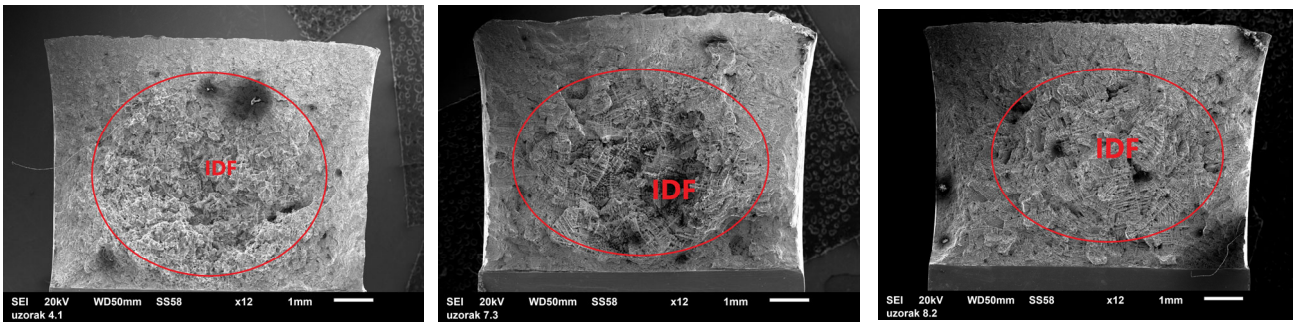
Figure 8. Force–time and energy–time diagrams for sample (3)–Mn16, WQA).

Table 3. Average values of energies, Ei, Ep, and Et.

Sample	Ei (J)	Ep (J)	Et (J)
4 Mn16V WQA	3.2 ± 0.2	16.3 ± 0.7	19.5 ± 0.9
7 Mn16 WQAA	4.7 ± 0.3	20.6 ± 1.2	25.3 ± 1.5
8 Mn16V WQAA	5.6 ± 0.2	14.7 ± 0.9	20.3 ± 1.1
3 Mn16 WQA	4.7 ± 0.6	21.5 ± 1.6	26.2 ± 2.2

3.2. Fractography

At low magnification, the fracture surface exhibits an overall brittle-like appearance, as shown in Figure 9. Narrow lateral shear zones with only minor plastic deformation are observed near the specimen edges, while a wide central fracture zone dominates the fracture surface. Within this central region, a pronounced dendritic morphology is clearly visible even at low magnification, indicating that the fracture behavior is strongly governed by the solidification structure of the material. A distinct crack initiation site cannot be clearly identified, suggesting that the fracture initiation was not localized but rather distributed across structurally weakened regions. The persistence of this dendritic solidification structure on the fracture surface (marked as IDF) further indicates that the applied heat treatment was insufficient to adequately eliminate the as-cast microstructural features, thereby promoting structurally controlled fracture under impact loading.



(**a**) (**b**) (**c**)

Figure 9. Fracture surfaces of Charpy specimens: (**a**) sample (4)–Mn16V, WQA; (**b**) sample (7)–Mn16, WAQQ; (**c**) sample (8)–MN16, WQAA.

At higher magnifications, the fracture surface of the Mn16V WQA sample exhibits a pronounced dendritic morphology, indicating that the crack propagation was strongly influenced by the as-cast solidification structure of the material, as shown in Figure 10a,b. The presence of clearly visible dendrite arms and interdendritic regions suggests that the fracture preferentially propagated along interdendritic zones, which are known to be chemically segregated and mechanically weakened due to the enrichment in carbon, manganese, and possible precipitates, as well as non-equilibrium phases. At higher magnifications, as shown in Figure 10c,d, limited plastic deformation is observed in the form of locally deformed ligaments between dendrite arms; however, the dominant fracture path follows interdendritic boundaries rather than transgranular microvoid coalescence. This behavior is typical of insufficiently homogenized Hadfield steel, where microsegregation and undissolved carbides reduce the impact toughness and promote structurally controlled fracture under dynamic loading. Except for local limited plastic deformation regions, microcracks are visible all over, indicating possible quasi-brittle mechanism.

Figure 11 shows fractography of the sample (7), Mn16 WQAA. Compared to the fracture surface, which represents specimen 4 alloyed with vanadium, dimples as indication of plastic deformation, observed in the immediate vicinity of the notch, are more pronounced. The remining fracture surface, similarly to the previous specimen, is characterized by an interdendritic fracture mechanism. The fracture of interdendritic ligaments can also be observed in the figure (marked).

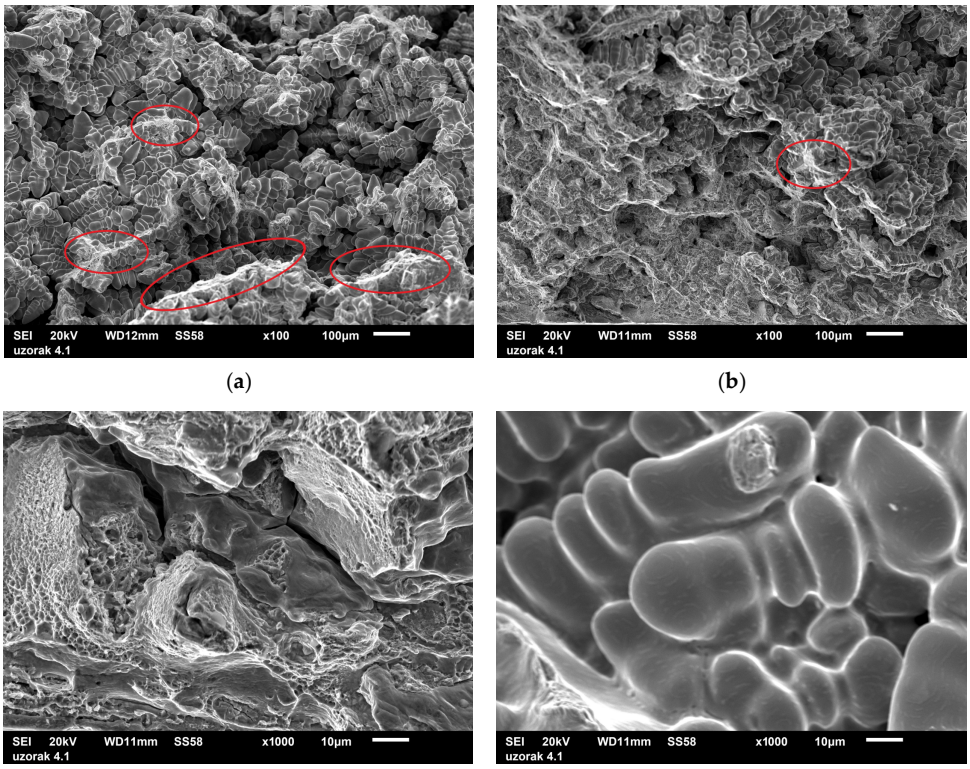


Figure 10. SEM fractography sample (4)–Mn16V WQA with dominant interdendritic fracture mechanism presented at various magnifications: (**a**,**b**) ×100 and (**c**,**d**) ×1000.

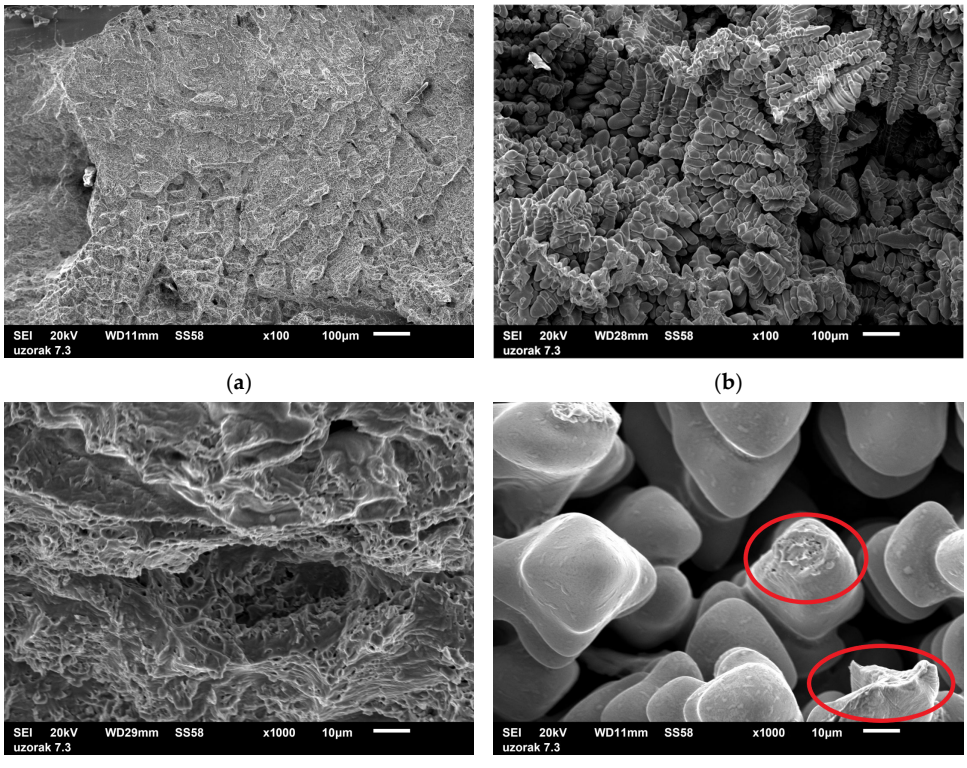


Figure 11. SEM fractography, sample (7)–Mn16 WQAA, indicating interdendritic fracture mechanism with more pronounced dimples presented at various magnifications: (**a**,**b**) ×100 and (**c**,**d**) ×1000.

4. Discussion

From total energy values, as shown in Table 2, one can see that samples (7) and (3), i.e., steel Mn16, have higher toughness than samples (4) and (8), i.e., Mn16V. This has confirmed the previously observed fact that V reduced the impact toughness of Hadfield steels. Nevertheless, one should keep in mind that the content of V was not the only difference in the chemical content between samples with and without V. Namely, in the case of Mn16V alloy content of Cr, Mo, and Ni is reduced and might also be influential to some extent.

Table 2 also indicates that the additional aging has had very little, if any, effect, since samples (3) and (7), representing Mn16 steel in WQA and WQAA states, have almost the same total energy values, as well as samples (4) and (8), representing Mn16V steel in the same way.

In terms of total energy values, one should also notice that they are not satisfying, since all of them are below 27 J, which is regarded as the minimum value for materials operating under impact loading [20–22]. This is also confirmed by fractography, revealing a brittle-like appearance with indications of plastic deformation on macro-scale, as well as dendritic and interdendritic fracture mechanism with a few dimples, indicating low toughness at the micro-scale. Previous research [18] published in paper showed that carbides are formed on grain boundaries. These results indicate that aging did not produce considerably finer microstructure, i.e., it can be assumed that primary carbides and dendrites present after quenching still played a dominant role in crack initiation and, respectively, low toughness. These grain boundary carbides are inherently brittle and act as preferential crack initiation sites, thereby facilitating intergranular fracture and reducing resistance to crack propagation. Their continuous or semi-continuous distribution along grain boundaries further promotes strain localization and premature failure under impact loading. Dendritic regions represent local chemical heterogeneities, which may lead to compositional gradients, uneven mechanical response, and localized stress concentration. The combined effect of brittle grain boundary carbides and dendritic segregation is therefore highly detrimental to toughness, as it promotes crack nucleation and accelerates unstable fracture propagation. Similar situation was observed in paper [9], where the failure analysis of excavator bucket tooth was performed. It was pointed out that improper heat treatment can cause brittle zones and reduce impact toughness significantly. The final conclusion was that two types of defects caused the failure, namely pores during casting and carbides left after dissolution treatment.

From Table 2, one can also see that the crack initiation energies are significantly smaller than the crack propagation energies for all samples, indicating high sensitivity of tested steels to cracking and somewhat better resistance to crack propagation. This behavior can be attributed to the presence of austenite in microstructure, i.e., FCC lattice which has good plasticity. This is certainly a better option for a cast ally, such as the Hadfield steel considered here. Namely, one should not rely on crack initiation energy for such a material, since it is common practice that micro-cracks will be present in its structure in any case.

5. Conclusions

Fracture behavior of Hadfield cast steels exposed to impact loading was investigated using two types of Hadfield steel, Mn16 and Mn16V and two heat treatments, WQA and WQAA. Based on the results of impact toughness obtained through the instrumented Charpy pendulum and fractography obtained through SEM, as presented here, one can conclude the following:

- The effect of vanadium on impact toughness of Hadfield steel is detrimental.
- The effect of additional aging on impact toughness of Hadfield steel is negligible.

- Total energy representing impact toughness is not satisfying, which is in agreement with the fractography indicating brittle-like fracture with low plasticity, as represented by a few dimples.
- Hadfield steel is more sensitive to crack initiation than to crack propagation under impact loading.

Author Contributions: Conceptualization, N.R. and A.S.; methodology, L.R. and A.V.; validation, A.S., S.D. and N.R.; formal analysis, A.V. and L.R.; investigation, A.V.; data curation, A.V., A.S. and S.D.; writing—original draft preparation, A.S. and S.D.; writing—review and editing, N.R. and L.R.; visualization, L.R. and S.D.; supervision, A.S. All authors have read and agreed to the published version of the manuscript.

Funding: This work was financially supported by the Ministry of Science, Technological Development and Innovation of the Republic of Serbia (Contract Nos. 451-03-137/2025-03/200325, 451-03-136/2025-03/200135 and 45103-136/2025-03/200213).

Data Availability Statement: The original contributions presented in this study are included in the article. Further inquiries can be directed to the corresponding author.

Conflicts of Interest: The authors declare no conflicts of interest.

Abbreviations

The following abbreviations are used in this manuscript:

SEM	scanning electron microscopy
WQA	water quenching and aging
WQAA	water quenching + aging + additional aging
WQ	water quenching

References

1. Subramanyam, D.K.; Swansieger, A.E.; Avery, H.S. Austenitic manganese steels. In *ASM Handbook*, 10th ed.; ASM International: Novelty, OH, USA, 1990; Volume 1, pp. 822–840.
2. Avery, H.S. *Austenitic Manganese Steel for Railway Trackwork*; Case Report No. 429-12; Abex Corporation Research Center: Mahwah, NJ, USA, 1981; 39p.
3. Avery, H.S. Austenitic manganese steel. In *Metals Handbook*, 8th ed.; American Society for Metals: Novelty, OH, USA, 1961; Volume 1, pp. 834–842.
4. Powell, G.W.; Marshall, E.R.; Backofen, W.A. Strain hardening of austenitic stainless steel. *Trans. Am. Soc. Met.* **1958**, *50*, 479–497.
5. Dastur, Y.N.; Leslie, W.C. Mechanism of work hardening in Hadfield manganese steel. *Metall. Trans. A* **1981**, *12*, 749–758. [CrossRef]
6. Drobnjak, D.; Parr, J.G. Deformation substructure and strain-hardening characteristics of metastable Fe−Mn austenites. *Metall. Trans.* **1970**, *1*, 759–765. [CrossRef]
7. Raghavan, M.J.; Sastri, A.S.; Marcinkowski, M.J. The nature of work hardening behaviour in Hadfield's manganese steel. *Trans. Metall. Soc. AIME* **1969**, *245*, 1568–1575.
8. Voort, G.V. (Ed.) *ASM Handbook, Volume 9: Metallography and Microstructures*; ASM International: Novelty, OH, USA, 2004.
9. Poser, M.; Zdraveski, F. Effect of casting and heat treatment on change in microstructure and mechanical properties in austenitic Hadfield steel. *Zavar. I Zavarene Konstr.* **2025**, *4*, 206–214. [CrossRef]
10. Youn-Soo, H.; Kim, J.T.; Kwak, S.Y.; Choi, J.K.; Yoon, W.Y. Critical cooling rate on carbide precipitation during quenching of austenitic manganese steel. *China Foundry* **2010**, *7*, 177–182.
11. Mahlami, C.S.; Pan, X. Mechanical properties and microstructure evaluation of high manganese steel alloyed with vanadium. *AIP Conf. Proc.* **2017**, *1859*, 020083. [CrossRef]
12. Bi, N.; Tang, H.; Shi, Z.; Wang, X.; Han, F.; Liang, J. Effects of Vanadium Microalloying and Intercritical Annealing on Yield Strength–Ductility Trade-Offs of Medium-Manganese Steels. *Materials* **2023**, *16*, 2220. [CrossRef] [PubMed]
13. Wang, R.; Zhang, W.; Zhang, F.; Fu, H.; Huang, Q.; Wu, H.; Li, Z.; Shan, Q. The effect of RRA treatment on mechanical properties and wear behavior in vanadium micro-alloyed Hadfield's steel. *J. Mater. Res. Technol.* **2023**, *24*, 9884–9896. [CrossRef]

14. Wang, J.; Bruel, G.; Wang, Z.; Gilbert, E.P.; Cizek, P.; Corujeira-Gallo, S.; Fabijanic, D.; Barnett, M. Hardening Due to Vanadium Carbides Formed During Short-Time Aging of Hadfield Steels. *Metall. Mater. Trans. A* **2023**, *54*, 1213–1222. [CrossRef]
15. Atasoy, I. Effect of alloying elements and heat treatment on the structure and properties of Hadfield's austenitic manganese steel. *Z. Metallkd.* **1984**, *75*, 463–471. [CrossRef]
16. Pribulová, A.; Babič, J.; Baričová, D. Influence of Hadfield's steel chemical composition on its mechanical properties. *Chem. Listy* **2011**, *105*, S430–S432.
17. Mahlami, C.S.; Pan, X. An overview on high manganese steel casting. In Proceedings of the World Foundry Congress, Bilbao, Spain, 19–24 May 2014.
18. Vukosavljević, A.; Sedmak, A.; Tadić, S.; Perković, S.; Radović, N. The effect of composition and heat treatment on impact toughness of Hadfield steel. *Tech. Gaz.* **2025**, *32*, 2217–2222.
19. Vukosavljević, A.; Sedmak, A.; Tadić, S.; Radović, L.J.; Radović, N. Composition and heat treatment effects on hardness and strength of a Hadfield steel. *Struct. Integr. Life* **2025**, *25*, 7–10. [CrossRef]
20. Kostić, N.; Čamagić, I.; Sedmak, S.; Burzić, Z.; Sedmak, A. Impact toughness of A516 Gr. 60 steel simulated heat-affected-zone. *Struct. Integr. Life* **2025**, *25*, 15–18. [CrossRef]
21. Perković, S.; Radaković, Z.; Burzić, Z.; Sedmak, S.; Sedmak, A.; Radović, L.J. Stress concentration effects on toughness value of duplex steel S32750. *Struct. Integr. Life* **2023**, *23*, 3–7.
22. Kostić, N.; Čamagić, I.; Sedmak, A.; Burzić, Z.; Sedmak, S.; Mandić, G.; Ostojin, M. Impact toughness behaviour of A516 Gr. 60 steel welded joints. *Struct. Integr. Life* **2024**, *24*, 232–239. [CrossRef]

Disclaimer/Publisher's Note: The statements, opinions and data contained in all publications are solely those of the individual author(s) and contributor(s) and not of MDPI and/or the editor(s). MDPI and/or the editor(s) disclaim responsibility for any injury to people or property resulting from any ideas, methods, instructions or products referred to in the content.